Electron-temperature and energy-flow history in an imploding plasma

L. Gregorian, E. Kroupp, G. Davara,* A. Starobinets, V. I. Fisher, V. A. Bernshtam, Yu. V. Ralchenko,† and Y. Maron
Faculty of Physics, Weizmann Institute of Science, Rehovot, 76100, Israel

A. Fisher
Faculty of Physics, Technion-Israeli Institute of Technology, Haifa, Israel

D. H. H. Hoffmann
Institut für Kernphysik, Technische Universität Darmstadt, 64289 Darmstadt, Germany
(Received 25 July 2004; revised manuscript received 28 January 2005; published 5 May 2005)

The time-dependent radial distribution of the electron temperature in a 0.6 μs, 220-kA gas-puff *z*-pinch plasma is studied using spatially-resolved observations of line emission from singly to fivefold ionized oxygen ions during the plasma implosion, up to 50 ns before maximum compression. The temperature obtained, together with the previously determined radial distributions of the electron density, plasma radial velocity, and magnetic field, allows for studying the history of the magnetic-field energy coupling to the plasma by comparing the energy deposition and dissipation rates in the plasma. It is found that at this phase of the implosion, $\sim$65% of the energy deposited in the plasma is imparted to the plasma radial flow, with the rest of the energy being converted into internal energy and radiation.

DOI: 10.1103/PhysRevE.71.056402 PACS number(s): 52.58.Lq, 52.30.Cv, 52.70.Kz

I. INTRODUCTION

The main objectives of the modern *z*-pinch research [1–8] are the enhancement of the plasma implosion uniformity and the efficiency of the magnetic energy coupling to the plasma. In the pursuit of these goals, efforts have been directed towards studying the energy flow in *z*-pinch devices, in particular by comparing the initial conditions of the plasma load to the x-ray emission characteristics during the stagnation phase of the plasma. In many such studies, however, it was found that the total measured x-ray radiation yield exceeds the calculated plasma kinetic energy by a factor of >2 [9,10]. These findings prompted numerous theoretical investigations (e.g., Ref. [11]) of possible anomalous energy deposition and dissipation mechanisms in the plasma during the implosion, still this energy balance problem is yet to be resolved.

As yet, due to a limited number of experimental studies, there is a little understanding of the magnetic energy coupling to the plasma during the implosion phase. In view of the difficulty outlined above, such a study of the time- and space-dependent properties of the imploding plasma can be highly useful for a fundamental understanding of the energy coupling at stagnation, and for the overall improvement of the *z*-pinch operation. In more detail, knowledge of the histories of parameters such as the particle temperatures and densities, current density, and ion velocity distribution is essential for studying the energy deposition and dissipation mechanisms, various transport processes, and the development of instabilities in the plasma during the implosion.

In an imploding plasma, the determination of the electron temperature T_e using spectroscopic measurements [12], requires addressing a few difficulties. First, the plasma flows across the line-of-sight of the spectroscopic system, so that the particles are replaced and the plasma properties vary during the observation time. Second, due to the plasma heating throughout the implosion, it continuously undergoes ionization so that the charge-state distribution and the line intensities also vary during the observation time. Furthermore, the electron density, the knowledge of which is required for the analysis of the line intensities, also varies in time both due to ionization and plasma compression. An additional difficulty in investigating such plasmas is caused by the shot-to-shot irreproducibility. Indeed, much effort has been devoted to assess the uncertainties in the measurements despite these difficulties, as is discussed below and in a companion paper [13].

In this study we report on the determination of T_e as a function of time and radial position within the imploding shell of a 0.6 μs, gas-puff *z*-pinch plasma for times up to 50 ns before stagnation. The temperature is obtained from measurements of line intensities of singly- to fivefold ionized oxygen ions, which are analyzed using time-dependent, collisional-radiative (CR) calculations [14]. The line-intensity ratios selected for the investigation are independent of the electron density n_e and the plasma-composition history, both of which are typically not known with sufficient accuracy in such transient plasmas. This allows for reducing the errors that result from the complications discussed in the above.

Using the radial distribution of the electron temperature obtained, together with the previously determined distributions of the particle velocities [15], magnetic field [16], and electron density [13], each of the energy deposition and dissipation rates in the plasma is calculated in a one-dimensional (1D) approximation. This allows for comparing

*Present adress: Orbotech Ltd., Yavne, Israel.

†Present address: Atomic Physics Division, NIST, Gaithersburg, Maryland 20899-8422.

the $\mathbf{J}\times\mathbf{B}$ work and the Joule heating to the kinetic and internal energies acquired by the plasma during the implosion and to the radiation emitted from the plasma. The partitioning of the $\mathbf{J}\times\mathbf{B}$ work into plasma pushing and compressional work is also obtained. These calculations also provide an examination of the consistency of the results described in the present report with all previous results obtained for this plasma. We thus believe that the data presented provide an experimental basis for detailed examinations of *z*-pinch modelling.

In the following, the *z*-pinch experiment and diagnostics are described in Sec. II, the measurements in Sec. III, and the argumentations for the data analysis in Sec. IV. The determination of the energy deposition and dissipation rates in the plasma is described in Sec. V.

II. EXPERIMENT AND DIAGNOSTICS

The experimental system used for the present study consists of a gas-puff device and a capacitor-bank discharge circuit (25 kV, $\simeq 0.01\Omega$, 1.2 μs 1/4 period) that delivers a current of $\sim$250 kA, driven axially through the cylindrical plasma. The operating gas, CO_2 in the present study, held at a plenum pressure of $\sim$50 psi, is released into the vacuum chamber through a 4-cm-diameter supersonic nozzle, forming a nearly annular gas shell across the 1.4-cm-long anode-cathode (*A*-*K*) gap. The anode is a copper-tungsten tube positioned co-axially in front of the nozzle (cathode). The peak gas density at $r=20$ nm, measured using an ionization-gauge probe for the axial positions between $z=10$ and 14 mm (where $z=0$ is the nozzle position), is $2.0\pm0.7\times10^{16}$ cm^{-3}, and the typical thickness of the gas shell is $\Delta r\sim 6$ mm [17]. The plasma implodes radially under the azimuthal magnetic field and stagnates on axis at $t=t_p\simeq 620$ ns (pinch time), where the total current at this time is $I_p\simeq 220$ kA. The reproducibility of the pinch time is within $\pm$20 ns.

The diagnostics consist of a 1.3-m spectrometer equipped with a 2400 grooves/mm grating, and a near-ultraviolet (NUV) streak camera lens-coupled to a cooled CCD (charge coupled device) that records the time-dependent spectra with a 1-ns resolution. The spectral range observed in a single discharge and the spectral resolution here used were $\simeq$7 Å and $\simeq$0.1 Å, respectively, the latter is much smaller than the typical widths of the line profiles observed (see Refs. [13,16]). Absolute calibrations of the system were performed periodically over the NUV and visible spectral regions. Among the levels used in the measurements described below (see Table I), certain population ratios, which are insensitive both to n_e and T_e in the plasma, were used for examining the relative calibration of the system. These were the population ratios of the level pairs $[3p\ ^2P]/[3p\ ^2D]$, $[3d\ ^3P]/[3d\ ^3D]$, $[3d\ ^4P]/[3d\ ^4F]$, and $[2p3p\ ^3P]/[2p3p\ ^3D]$ of O II, O III, O IV, and O V, respectively.

The plasma was observed in the *z* direction with the line of sight at various radial positions. The image of the spectrometer input slit at the plasma plane, defining the volume viewed, was typically 1-mm wide (in the radial direction) and 2.5-mm high (in the azimuthal direction). The integration length along the line of sight was $\simeq$4 mm, since this is the length of the plasma column, located near the anode side of the *A*-*K* gap, which was observed to implode uniformly and earlier than the rest of the column [17]. Within this region, the plasma parameters varied little along the axial position *z* [13,16], therefore not affecting the accuracy of the measurements here described.

TABLE I. The spectral lines used in the measurements, together with the parameters of the transition upper levels and the transition Einstein coefficients.

Charge state	λ (Å)	Upper level configuration	Upper level energy (eV)	A_{ul} (10^8 s^{-1})
O II	4349.43	$3p\ ^4P_{5/2}$	25.85	0.68
	4345.56	$3p\ ^4P_{5/2}$	25.85	0.68
O II	4347.43	$3p\ ^2D_{3/2}$	28.51	0.94
	4351.27	$3p\ ^2D_{5/2}$	28.51	0.99
O II	3911.96	$3p\ ^2P_{3/2}$	28.83	1.09
O II	4132.81	$3d\ ^4P_{3/2}$	28.83	0.84
O II	4189.79	$3d\ ^2G_{9/2}$	31.32	1.98
O III	3759.87	$2p3p\ ^3D_3$	36.48	0.98
O III	3047.13	$2p3p\ ^3P_2$	37.25	1.49
O III	3017.63	$2p3d\ ^3D_3$	40.58	0.54
O III	3444.10	$2p3d\ ^3P_2$	40.85	0.42
O IV	3063.47	$3p\ ^2P_{3/2}$	48.38	1.31
O IV	3411.69	$3d\ ^2D_{5/2}$	52.02	1.02
O IV	3385.55	$2s2p(^3P)3p\ ^4D_{7/2}$	58.12	1.02
O IV	3736.85	$2s2p(^3P)3d\ ^4F_{9/2}$	61.43	0.80
O IV	3375.40	$2s2p(^3P)3d\ ^4P_{5/2}$	62.50	0.76
O V	2781.03	$2s3p\ ^3P_2$	72.27	1.40
O V	3144.68	$2s3d\ ^1D_2$	75.95	0.91
O V	4123.96	$2p3p\ ^3D_3$	84.02	0.48
O V	2755.13	$2p3p\ ^3P_2$	85.51	1.38
O VI	3811.35	$3p\ ^2P_{3/2}$	82.61	0.51

The plasma implosion uniformity in the azimuthal direction was examined by comparing line intensities and spectral widths observed for different azimuths at different discharges. Variations of up to 10% in the statistically-averaged intensities and up to 5% in the averaged widths were seen, both being within the experimental uncertainties due to discharge irreproducibilities quoted below.

III. MEASUREMENTS

In the present study, the electron temperature is determined from the analysis of various T_e-sensitive population ratios of ionic energy levels, which in the case of an optically thin plasma are obtained from observations of emission-line intensities from different ion species. Specifically, the relation between the population ratio of the upper levels u_1 and u_2 of the transitions 1 and 2 within a given charge state to the ratio of the corresponding wavelength-integrated line inten-

sities I_1 and I_2, emitted from the same plasma region, is given by

$$\frac{n_{u_1}}{n_{u_2}} = \frac{I_1/[g_1 A_1 K(\lambda_1)]}{I_2/[g_2 A_2 K(\lambda_2)]}. \quad (1)$$

Here, A_i is the probability of spontaneous radiative transition, g_i is the upper-level degeneracy ($g=2J+1$), and $K(\lambda)$ is the system sensitivity due to the geometric light-collection efficiency and the system absolute response. The line intensities are given in units of photons/(sr·s·cm^2). Throughout the paper n_u is the level population divided by the degeneracy.

In order to correctly determine the electron temperature in the plasma, several criteria were required to be met in selecting the most suitable transitions and level-population ratios. First, lines of oxygen ions were chosen within spectral intervals which are free of impurity lines of carbon, copper, and tungsten, the latter two originating at the electrodes. Time-dependent collisional-radiative calculations (see Sec. IV A below) were then performed in order to estimate the line intensities and opacities, using the expected plasma parameters based on the previously observed charge-state radial distribution [15] and continuum radiation emission [13]. The opacity calculations are described in Sec. IV B below. In addition, the transitions selected here were between sufficiently high-lying levels, for which the population ratios are insensitive to the ionization into the respective charge state (but not too high to be affected by recombination).

At a certain radial position of observation both the electron density n_e and the plasma charge-state composition vary in time due to ionization and the plasma flow across the line of sight. Moreover, the histories of both parameters are not known with sufficient accuracy in our plasma. Therefore, only T_e-dependent level population ratios that are least sensitive to n_e and to the composition were selected amongst the transitions given in Table I.

The time-dependent measurements were carried out at several radial positions between $r=6.0-20.0$ mm using spectral lines of the dominating charge states for the different times and radii, as known from the observed time-dependent radial distribution of charge-state density in the plasma [15], an example of which is shown in Fig. 1. Specifically, for $t=490$ ns O II lines were observed at $r=12.0$ mm, and O IV and O V lines at $r=16.5$ mm. For $t=535$ ns, O II, O III, and O IV lines were observed at $r=8.0$, 9.0, and 10.5 mm, respectively, while lines of both O V and O VI were observed at 12.0 mm. For $t=570$ ns, lines of both O V and O VI were observed at $r=8.0$ mm. For each position, the spectra are recorded as a function of time, typically using 4–8 discharges for each line, in order to average over shot-to-shot variations up to a factor 3 in the intensity and ±10 ns in the time of peak line emission.

Figure 2 gives an example of time-dependent line intensities from successive charge states, observed at $r=16.7$ mm. In the figure, the relative delay between the peak intensities of the lines of O II, O III, and O IV is due to the radial propagation of an ionization front that is faster than the radial ion motion. A detailed discussion of this phenom-

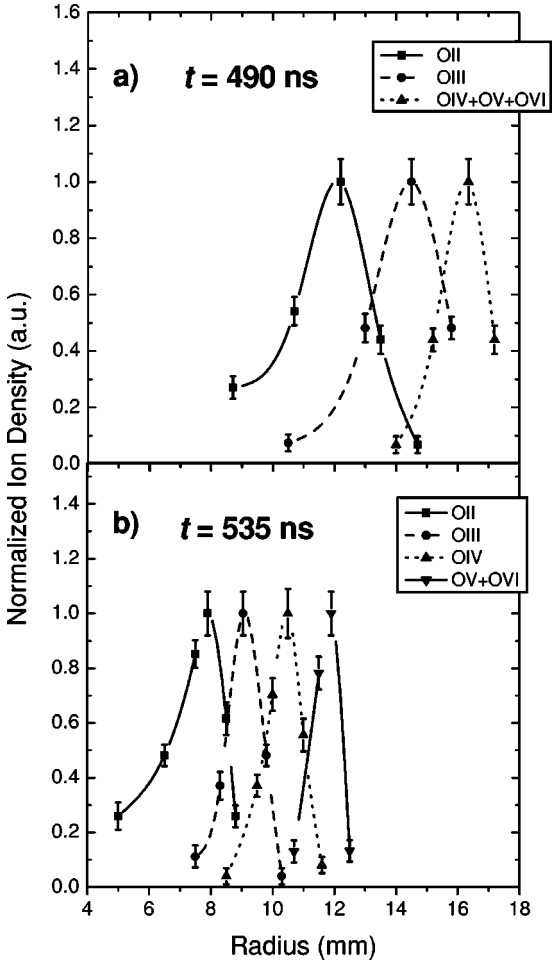

FIG. 1. Radial distribution of the ion charge state across the plasma at $t=490$ ns (a) and at $t=535$ ns (b), obtained from the relative line-emission intensities as observed at several radial positions. The peak density of each charge state is assumed to be unity.

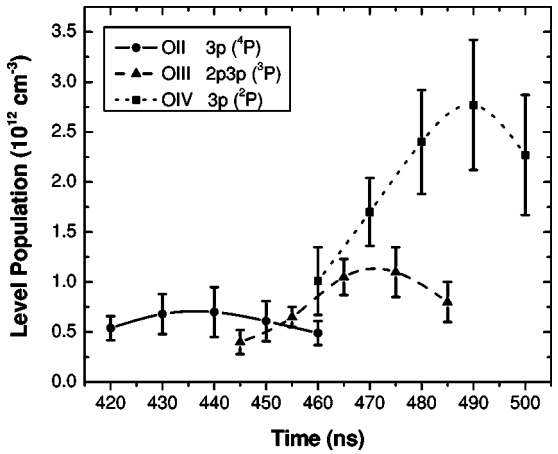

FIG. 2. Examples of the time-dependent population of various levels obtained from end-on observations at $r=16.7$ mm. Solid line: O II $3p\ ^4P_{5/2}$ level (4349.43 Å); Dashed line: O III $3p\ ^3P_2$ level (3047.14 Å); Dotted line: O IV $3p\ ^2P_{3/2}$ level (3063.5 Å).

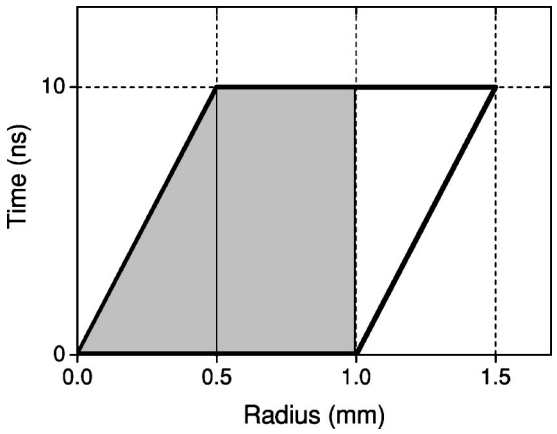

FIG. 3. A schematic of the particle flow through a 1-mm-wide plasma slab during a 10 ns observation interval (see text). The grey area represents the radiation yield of the outgoing particles.

enon, previously observed for the plasma under study [15], is given in Ref. [13]. It should be emphasized that the level populations given throughout the paper correspond to the times of the peak respective line intensities, since for any given radius the times of peak intensity were found to be the same for all lines of a given charge state.

IV. DATA ANALYSIS AND RESULTS

A. Collisional-radiative modeling

The time-dependent CR calculations used for the data analysis are described in Ref. [14]. In brief, the modeling is based on the solution of the time-dependent rate equations

$$\frac{d\hat{N}(t)}{dt} = \hat{A}(n_i, n_e, T_e)\hat{N}(t) + \hat{S}(t), \tag{2}$$

where $\hat{N}(t)$ is the vector of atomic state populations (i.e., the number of ions per quantum state in a small volume δV within which the plasma parameters are assumed to be uniform), $\hat{A}(n_i, n_e, T_e)$ is the rate matrix, and $\hat{S}(t)$ is the source function that simulates an external supply of particles into δV. The quantities n_i, n_e, and T_e are time-dependent input parameters. In the calculations, n_e is consistently equal to $\Sigma_\alpha Z_\alpha n_i^\alpha$, where α is the ionization stage.

The rate matrix accounts for the following processes: electron impact excitation and de-excitation, electron impact ionization (both single and multiple), radiative and 3-body recombinations, and spontaneous radiative decay. While the kinetic modelling allows for the use of arbitrary electron energy distribution functions, Maxwellian-averaged rates are used in the present study. The atomic data used here were both calculated and obtained from databases [18–21].

The plasma self-absorbtion is treated within the escape factor formalism [22]. For each line studied the optical thickness τ and the escape factor Θ [23] are calculated based on the expected plasma conditions [13,15], and the known plasma geometry. The line widths required for the opacity calculations are obtained using the Voigt line profiles that result from the electron-impact Stark broadening and the thermal Doppler broadening. For the Doppler broadening we assume an ion temperature $T_i = T_e$, however the calculated opacity effects were found to be insensitive to this assumption due to the dominance of the electron-impact broadening.

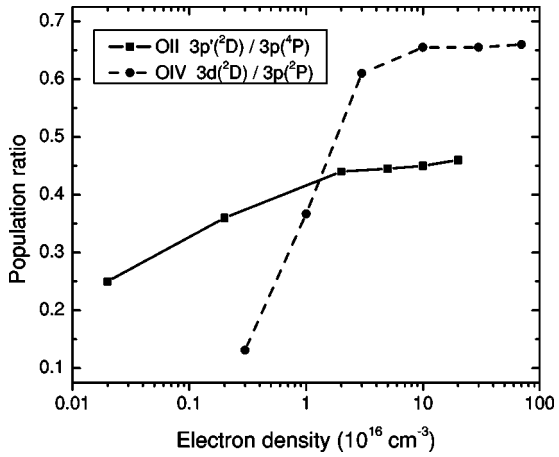

FIG. 4. Dependence of the O II $[3p'\ ^2D]/[3p\ ^4P]$ and the O IV $[3d\ ^2D]/[3p\ ^2P]$ population ratios on n_e, calculated using fixed T_e values of 5 and 9 eV for O II and O IV, respectively.

B. Determination of the electron temperature

The analysis of the experimental data is based on the comparison between the level-population ratios, obtained from the measured line intensities using Eq. (1), to those calculated using the CR modeling, in which T_e is used as an input parameter. The modeling does not assume a collisional-radiative equilibrium (CRE), i.e., the level populations are calculated as a function of time. The analysis procedure is performed separately for each experimental data point in (r,t), and the value of T_e that yields the best agreement in such comparisons gives then the local instantaneous electron temperature $T_e(r,t)$. In the following, we discuss the various assumptions underlying this analysis procedure.

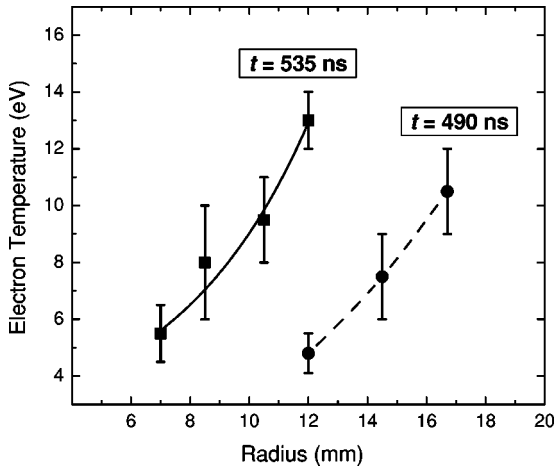

FIG. 5. Radial distribution of the electron temperature in the plasma for two times during the implosion, obtained from end-on observations of line-intensity ratios for O II–O VI ions.

TABLE II. Experimental and calculated populations of O II levels, normalized to the population of the O II $2p^2(^3P)3p\ ^4P$ level, given for three instants during the plasma implosion. t_p is the time at which the peak line-intensities are observed at the respective radial position r.

t_p (ns), r (mm)	n_e (10^{17} cm^{-3})	Level configuration	Measured population	Calculations		
				4 eV	5 eV	6 eV
440	1.5	$3p'\ ^2D$	0.50±0.15	0.45	0.54	0.62
16.5		$3d\ ^4P$	0.48±0.11	0.445	0.53	0.60
		$3p'\ ^2P$	0.44±0.11	0.445	0.55	0.64
490	1.0	$3p'\ ^2D$	0.53±0.11	0.45	0.54	0.615
11.7		$3p'\ ^2P$	0.48±0.12	0.44	0.55	0.64
535	0.5	$3p'\ ^2D$	0.63±0.15	0.445	0.535	0.61
7.7		$3d'\ ^2G$	0.17±0.03	0.14	0.18	0.205

As said above, the main difficulties in analyzing data obtained in an imploding plasma are the radial flow of the plasma across the line of sight and the continuous ionization, which cause uncertainties in the line intensities observed due to the variation in time of T_e, n_e, and the mean charge Z. The effect of these complications on the level-population ratios here used was examined using CR calculations. First, let us estimate the effect of the particle replacement in the 1-mm-wide radial plasma region observed caused by the plasma radial flow. Since the typical particle radial velocities are $\sim 5\times 10^6$ cm/s [15], ~50% of the particles are replaced during the 10-ns observation time. However, the incoming particles contribute only ~25% of the total radiation emitted from the region observed, as illustrated in Fig. 3. We may thus assume that variation in the parameters during the observation time is mainly due to the evolution for the same group of particles rather than to the plasma replacement. An additional support to the neglect of the particle replacement effect is that in the present experiment all the gradient length scales in the plasma are found to be larger than 0.5 mm (see Fig. 5 below and Refs. [13,16]). This value is comparable to the flow velocity times the observation time interval.

The values of n_e used for the analysis are obtained from Refs. [13,24] based on measurements of continuum radiation and absolute line intensities, respectively. The dependence of the level-population ratios used on n_e was found to be negligible, with variations of $\leqslant$5% obtained for the entire range of n_e in the plasma (2×10^{16}–2×10^{18} cm^{-3}). For example, given in Fig. 4 are the O II $[3p'\ ^2D]/[3p\ ^4P]$ and the O IV $[3d\ ^2D]/[3p\ ^2P]$ ratios as a function of n_e. The variations due to n_e are thus well within the experimental uncertainties quoted below, which justifies the use of constant values of n_e in the calculations.

The effect of the temperature variation during the 10-ns observation interval for a given radial position, both due to the time evolution of T_e within the volume observed and the radial plasma flow, was examined based on the equilibration times of the upper level populations within the same charge state. It was verified that for the present plasma parameters all the population ratios chosen here reach steady values in less than 2 ns. Therefore, measurements of line-intensity ratios at any given radial position yields the local, instantaneous value of T_e, independent of the T_e history at different locations.

In the analysis of the data for each r and t constant values of T_e are assumed. It will be shown *a posteriori* that this assumption is justified based on the dependencies of T_e on the radius and time obtained. In more detail, the variations of T_e within the spatial and temporal resolution elements of the measurements were found to be smaller than the uncertainties in T_e quoted below, the latter mainly resulting from the uncertainties in the measured line intensities.

The level-population ratios of a given charge state may be affected by the ionization into that charge state. For estimating the uncertainty due to this effect the level-population ratios of the various charge-state ions were calculated using different source functions for the ground states of the given ions. We first note that for each radial position the duration of the domination of each charge state is longer than 10 ns. Assuming in the calculations an instantaneous source of ions at the ground state of a certain ionization stage (here denoted by a δ-source function), we found that the level-population ratios within each charge state reach steady values in less than 10 ns, even though the ionization processes are slower (i.e., the charge state distribution changes over a longer time scale). This result was not affected by assuming other source functions in the calculations for the various charge states. It was also found that for all charge states, variations of ±25% in Z yield uncertainties of $<$2% in the calculated level-population ratios used here for the determination of T_e. Since for the times studied here the rise of Z within the plasma region observed during a 10-ns interval was shown to be small ($<$10%) [15], it can be concluded that the plasma ionization does not affect the results given below.

In the calculations of the self-absorbtion effects on the level populations of a given charge state, the photon escape length was chosen to be half the radial width of the region occupied by that charge state. The typical values of this length for the times studied here are $\simeq$1.5 mm (see Fig. 1). In the calculations, the ion temperature T_i is assumed to be equal to T_e. Based on this assumption, the validity of which

TABLE III. Experimental and calculated level-population ratios of O III, given for $t_p = 535$ ns and $r = 8.8$ mm.

n_e (10^{17} cm^{-3})	Level configuration	Measured ratio	Calculations			
			7 eV	8 eV	9 eV	10 eV
1.5	$3d\,^3D/3p\,^3D$	0.70±0.06	0.60	0.66	0.715	0.77
	$3d\,^3P/3p\,^3D$	0.76±0.09	0.53	0.59	0.63	0.665
	$3d\,^3D/3p\,^3P$	0.60±0.11	0.605	0.64	0.67	0.695
	$3d\,^3P/3p\,^3P$	0.64±0.10	0.535	0.57	0.59	0.605

is examined in the following section, all the lines used in the measurements (Table I) were found to be optically thin ($\tau < 0.1$). Further calculations using T_i varying between $0.1T_e$ to $10T_e$ showed that the resultant variations in τ obtained for the various transitions had a negligible effect on the level population ratios here discussed. For the transitions between low-lying energy levels, the calculated optical thickness was found to affect the mean charge Z and the upper level populations. However, the effects of these opacities on the upper-level population ratios as well as on the ionization rates in the plasma were found to be negligible.

The effect of the opacity was also examined experimentally, by comparing the intensities of simultaneously-observed lines originating at the same upper level of a given charge state, for example, the O II 4349.43-Å and 4345.56-Å lines originating at the $3p\,^4P$ level, and the 4351.27-Å and 4347.43-Å lines originating at the $3p'\,^2D$ level. For each pair of transitions, the level populations obtained from the measured intensities of the two lines were found to agree to within ~15%. Since this value is less than the experimental uncertainty of each line intensity, it may be used to confirm the optical thinness for these lines.

In the present work, only a single emission line was observed in a single discharge. The line intensities, measured at the time of peak emission of the respective charge state for a given radial position, varied in the experiments by up to ×3. These variations mainly resulted from the irreproducibility in the ion (and electron) density, as shown from continuum measurements [13], and confirmed by appropriate CR calculations. For this reason we used the following procedure for determining the average population ratio for two given ionic levels: The higher population densities observed for one level were divided by the higher densities observed for the other level, and averaging of all ratios obtained was made. The scattering of the ratios around the average value yielded the uncertainty in the ratio. We note that this averaging procedure was not required for the ratios of O II, since the data for O II were highly reproducible (intensity variations of <20%).

The experimental data, together with the results of the CR calculations for several values of T_e, are presented in Tables II–V. As said above, for each charge state only population ratios that were found to be weakly-dependent on n_e and on the charge-state composition were selected. In order to improve the accuracy in the determination of T_e, 2–4 population ratios were used for each charge state. The results are also examined by performing consistency checks with the particle ionization times, independently determined for any given r and t, as described below (see Table VI). This examination helps to discard T_e values obtained from experimental population ratios that particularly suffer from poor statistics or discharge irreproducibilities.

Table II gives the comparison between the level populations of O II, all normalized to the population of the $3p\,^4P$ level, measured at $t = 440$, 490, and 535 ns, and the calculated ratios. In this table, the populations of the $3p'\,^2D$ and $3p\,^4P$ levels are obtained using the averaged results of the corresponding pair of lines (see Table I). For $t = 440$ ns, it is seen that $T_e = 4.5 \pm 0.5$ eV gives population ratios that fit, within the error bar, all three ratios measured. Similarly, $T_e = 4.8 \pm 0.7$ eV and 5.5 ± 1.0 eV are seen to fit best the data for $t = 490$ and 535 ns, respectively.

Table III gives the results for O III. Here, the comparison between the population ratios measured at $t = 535$ ($r = 8.8$ mm) to the calculations yields a temperature of

TABLE IV. Experimental and calculated level-population ratios of O IV, given for two instants during the plasma implosion.

t_p (ns), r (mm)	n_e (10^{17} cm^{-3})	Level configuration	Measured ratio	Calculations			
				8 eV	9 eV	10 eV	11 eV
490	4.0	$3d\,^2D/3p\,^2P$	0.62±0.08	0.625	0.655	0.68	0.70
16.5		$3d\,^4F/3p\,^4D$	0.69±0.07	0.65	0.675	0.70	0.72
		$3d\,^4P/3p\,^4D$	0.65±0.08	0.56	0.595	0.62	0.64
535	3.0	$3d\,^2D/3p\,^2P$	0.67±0.11	0.625	0.655	0.68	0.70
10.2		$3d\,^4F/3p\,^4D$	0.57±0.08	0.65	0.675	0.70	0.72
		$3d\,^4P/3p\,^4D$	0.62±0.10	0.56	0.59	0.615	0.64

TABLE V. Experimental and calculated level-population ratios of O V, given for three instants during the plasma implosion. Also given is the population ratio of O VI to O V levels for $t=570$ ns.

t_p (ns), r (mm)	n_e (10^{17} cm^{-3})	Level configuration	Measured ratio	Calculations			
				11 eV	12 eV	13 eV	14 eV
490, 16.5	4.0	$2p3p\ ^3P/2s3d\ ^1D$	0.33±0.05	0.33	0.35	0.37	0.39
535	7.0	$2s3d\ ^1D/2s3p\ ^3P$	0.63±0.07	0.69	0.71	0.72	0.73
12.0		$2p3p\ ^3P/2s3p\ ^3P$	0.27±0.04		0.255	0.27	0.285
		$2p3p\ ^3P/2s3d\ ^1D$	0.42±0.05		0.36	0.38	0.40
570	20.0	$2s3d\ ^1D/2s3p\ ^3P$	1.01±0.30	0.71	0.73	0.735	0.735
7.5		$2p3p\ ^3P/2s3p\ ^3P$	0.62±0.28		0.30	0.32	0.345
		$2p3p\ ^3P/2s3d\ ^1D$	0.51±0.11	0.39	0.415	0.445	0.47
570	20.0	O VI $3p\ ^2P/$O V $2s3p\ ^3P$	3.6±2.1		2.1	5.0	9.75
7.5		O VI $3p\ ^2P/$O V $2s3d\ ^1D$	5.15±3.4		2.9	6.5	13.3

8.0±2.0 eV, which is seen to fit the data reasonably well. Based on the particle ionization times (Table VI) we discarded the results for the $[2p3d\ ^3P]/[2p3p\ ^3D]$ and the $[2p3d\ ^3P]/[2p3p\ ^3P]$ ratios, which both give large deviations in the value of T_e, probably due to a large experimental uncertainty in the population of the $2p3d\ ^3P$ level.

Table IV gives the comparison between the measured and the calculated level-population ratios for O IV. The experimental data are obtained for $t=490$ and 535 ns, and $r=16.5$ and 10.2 mm, respectively. It is seen that temperatures that provide reasonable fits to the data, to within the uncertainty in each ratio, are $T_e=10.0\pm2.0$ and 9.5±1.5 eV for the two times, respectively. As an example of using the ionization times in examining the values of T_e obtained from certain ratios, we note that a value of 0.57 for the $[3d\ ^4F]/[3p\ ^4D]$ ratio for $t=535$ ns requires $T_e\simeq6$ eV. However, such a value of T_e gives an ionization time >200 ns for O IV, much longer than the experimental ionization time (~25 ns). Indeed, this value of 0.57, is much lower than the other two ratios obtained for $t=535$ ns.

Table V gives the comparison between the experimental population ratios of O V obtained for $t=490$, 535, and 570 ns, to the ratios calculated using various values of T_e. At $t=490$ ns, the temperature was determined using a single ratio, $[2p3p\ ^3P]/[2s3d\ ^1D]$, since the data for the other level populations of O V was relatively uncertain and irreproducible, probably due to the proximity of this measurement to the time of the initial observation of O V lines in the plasma ($t\simeq480$ ns). It is seen that for this ratio, $T_e=11.0\pm2.0$ eV fits the data well. For this time, O V and O IV are observed to share the same radial position (Fig. 1), and it is seen that this temperature agrees well with T_e obtained using lines of O IV (10.0±2.0 eV). It is then quite reasonable to assume that the same temperature of 10.5±1.5 eV is common to both charge-state "clouds." At $t=535$ ns, a temperature of 13.0±2.0 eV is seen to fit the data reasonably well, except for the $[2s3d\ ^1D]/[2s3p\ ^3P]$ which gives $T_e<9$ eV, a value much lower than expected for this plasma (see Table VI). The inconsistency for this ratio is attributed to insufficient statistics. At $t=570$ ns the large uncertainties in the population ratios, as seen in Table V, are due to the much less reproducible line intensities (variations of up to factor 3) for this time of the implosion. We note that no reliable line-intensity data could be obtained for the plasma here studied for later times. As seen in the table, the only useful population ratio at this time is the $[2p3p\ ^3P]/[2s3d\ ^1D]$ ratio, which together with the bounds on T_e (Table VI), gives $T_e=14.0\pm2.0$ eV. The values of each of the other two ratios are higher by at least 40% than the theoretical values for $T_e=14$ eV. Such values of T_e are unreasonably too high, for example, for $T_e=16$ eV the ionization time of O V is ~5 ns, much less than the observation duration (~20 ns) of the O V lines at $r=7.5$ mm.

TABLE VI. Determination of the electron-temperature range from the observed ionization times of the different charge-states (defined as the times of an e-fold drop in the charge-state density).

Charge state	n_e (cm^{-3})	T_e range (eV)
O II	2×10^{16}–2×10^{17}	4.0–6.0
O III	5×10^{16}–5×10^{17}	6.0–9.0
O IV	1×10^{17}–1×10^{18}	9.0–12.0
O V	1×10^{17}–2×10^{18}	11.0–15.0

As said above, the expected range of T_e values for each charge-state-dominated plasma region is independently determined from comparisons between the observed ionization times of the various charge states to those obtained from CR calculations using variable input values for T_e and n_e. The results for the various charge states are summarized in Table VI.

In a plasma region which contains several charge states, measurements of population ratios of levels belonging to dif-

TABLE VII. Comparison between the time-dependent experimental ratios of O VI to O V level populations, measured at $r=12.0$ mm ($t_p=535$ ns), and the ratios calculated using $n_e=7\times10^{17}$ cm^{-3}.

Level configuration	Measurements		Calculations			
	time (ns)	ratio	time (ns)	12 eV	13 eV	14 eV
$3p\ ^2P/2s3d\ ^1D$	t_p-10	1.96	5	0.16	0.35	0.65
	t_p	3.46	15	0.88	1.96	3.95
	t_p+10	3.86	25	1.78	4.17	8.93
$3p\ ^2P/2s3p\ ^3P$	t_p-10	1.73	5	0.12	0.26	0.49
	t_p	2.27	15	0.62	1.40	2.81
	t_p+10	2.83	25	1.22	2.86	6.00

ferent charge states yield higher accuracy in the determination of T_e due to the high sensitivity of such ratios to T_e. However, in a rapidly ionizing plasma these ratios are highly time-dependent, thus requiring a careful data analysis. Here, we use the data obtained for O V and O VI, namely, the population ratios of the O VI $3p\ ^2P$ level to the O V $2s3p\ ^3P$ and $2s3d\ ^1D$ levels, which are observed at the same radial positions at $t=535$ and 570 ns, in order to verify the values of T_e obtained from the O V ratios for both instants. At each radial position, lines of the two charge states are measured during a 20-ns time interval, yielding population ratios at $t=t_p-10$ ns, t_p, and t_p+10 ns, where t_p is the time of peak line intensity.

An example for such an analysis for $t=535$ ns is given in Table VII. The measured values of both the $[3p\ ^2P]/[2s3p\ ^3P]$ and the $[3p\ ^2P]/[2s3d\ ^1D]$ ratios are compared to the ratios obtained from CR calculations for $t=5$, 15, and 25 ns (here $t=0$ is the calculation start time). In the calculations, T_e, n_e, and the number of particles are all assumed to be constant in time. It is seen that both calculated ratios rise in time faster than the experimental ratios. This can be explained by the continuous rise in the O V inventory within the observed plasma region during the observation time interval due to the mass sweeping. It is seen from this comparison that a temperature between 13.0–14.0 eV fits the data well, which is in a good agreement with the results for the O V ratios (Table V).

At $t=570$ ns, the insufficient accuracy in the data at t_p-10 ns and t_p+10 ns, did not allow for such a time-dependent analysis to be carried out, however the instantaneous ratios at t_p could still provide an estimate for T_e. The measured ratios, together with the calculated ones are given in Table V. A temperature of 13.0 ± 1.0 eV gives a reasonable fit of the data, also consistent with the result of the O V $[2s3d\ ^1D]/[2s3p\ ^3P]$ ratio for this time (see Table V).

Figure 5 gives the radial distribution of T_e at $t=490$ and 535 ns, using the results given in Tables II–V above. The value of T_e given at $t=490$ ns for the radial position of O III ($r=14.5$ mm) is obtained from interpolation based on the ionization times, since for this time and radial position no reliable data of line-intensity ratios were available. As shown in the figure, simple smooth curves through the data points are used to fit the data. It can be seen from these distributions, and from the additional data points for O II at $t=440$ ns and for O V–O VI at $t=570$ ns, that during the ~100-ns interval of the most significant plasma radial motion, the rise in the electron temperature is small, both at the colder (inner) boundary (from 4.5 to 5.5 eV) and at the hotter (outer) boundary (from 10.5 to 13–14 eV).

In addition to the uncertainties in the data and in the analysis discussed above, we now evaluate the effect of the uncertainties in the modeling on the values of T_e obtained. Specifically, we examined the sensitivity of T_e to uncertainties in the cross sections of the various processes included in the CR calculations, the upper limit for which, for example in the case of O IV and O V is ~20% [25]. To this end, we calculated the level population ratios for O IV and O V using the same plasma conditions as above, with all the collisional excitation and de-excitation cross sections smaller or larger by 20% (with the decay rates A_{ik} remaining unchanged). The resulting variations in the level population ratios were found to be $\leqslant3\%$, corresponding to uncertainties of up to ±0.5 eV in T_e (i.e., within the uncertainties quoted in the above).

V. DISCUSSION

The electron temperature obtained above, together with the results for the electron density [13], the ion velocity and charge-state distributions [15], and the magnetic-field distribution [16], allow for analyzing the energy balance in the plasma during the implosion. Knowledge of the time-dependent radial distributions of the energy deposition and dissipation mechanisms is required for tracking the history of the energy and momentum within a given plasma cell (a Lagrangian cell), in order to better understand the internal energy dynamics across the plasma shell.

Assuming that the dependence on the axial (z) and azimuthal (θ) coordinates is negligible, we use a one-dimensional (1D) single-fluid, single-temperature ($T_e=T_i=T$), magnetohydrodynamic (MHD) model to describe the plasma under study. Following Ref. [26], the equation for the total (internal and kinetic) energy per unit mass can be derived:

$$\frac{d}{dt}\left(\varepsilon+\frac{v^2}{2}\right)=-\frac{1}{\rho r}\frac{\partial}{\partial r}(rpv)+\frac{1}{\rho r}\frac{\partial}{\partial r}\left(r\kappa\frac{\partial T}{\partial r}\right)+\frac{1}{\rho}\eta J_z^2-\frac{v}{c\rho}J_zB_\theta+\dot{\varepsilon}_{\mathrm{rad}}. \quad (3)$$

Here, $d/dt=\partial/\partial t+v(\partial/\partial r)$, ρ is the plasma mass density, v

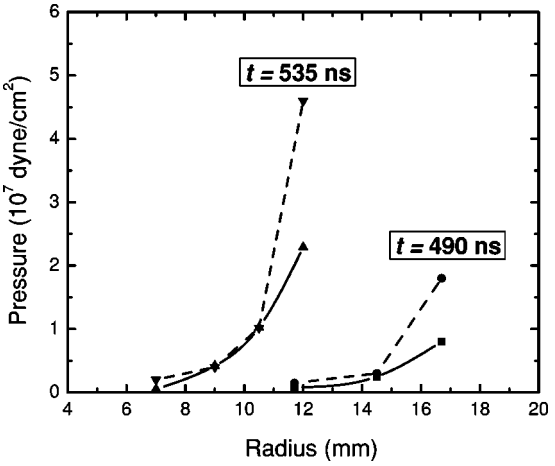

FIG. 6. Radial distributions of the thermal pressure (solid line) and the magnetic pressure (dashed line) for two times during the implosion.

$=v_r$ is the radial velocity of the plasma flow, p is the thermal pressure, $J_z=(c/4\pi r)\partial(rB_\theta)/\partial r$ is the axial current density (where B_θ is the azimuthal magnetic field), and $\dot{\varepsilon}_{\rm rad}$ is the radiation cooling rate. η is the electrical resistivity, here assumed to be the Spitzer resistivity [27], and $\kappa \simeq \kappa_e$ is the thermal conductivity [28]. The specific internal energy ε includes the thermal, ionization, and excitation energies. Calculations of the right-hand-side (RHS) terms in Eq. (3) are described in the following section.

Let us first examine the assumption of a single plasma temperature by calculating the particle collision rates in the plasma. More specifically, we use the characteristic energy-transfer time for electron-ion collisions [28]

$$\tau^\epsilon = (1/\tau^\epsilon_{ei} + 1/\tau^\epsilon_{ie})^{-1} = \frac{3.125\times 10^8 \mu T_e^{3/2}}{(1+Z)Z\ln\Lambda n_e}\ \text{s}, \qquad (4)$$

where μ is the ion mass in proton-mass units and $\ln\Lambda$ is the Coulomb logarithm. Using the radial distributions of T_e, n_e, and Z, Eq. (4) gives a typical value of $\tau^\epsilon \simeq 10$ ns for the entire shell, which is much shorter than the time scale of the T_e changes in the plasma ($\simeq 1$ eV over ~ 30 ns).

The thermal pressure $p=p_e+p_i$ is obtained from the particle densities and temperatures, again assuming $T_i=T_e$. A comparison between the radial distribution of p with that of the magnetic pressure $B^2/8\pi$ for two times during the implosion is given in Fig. 6. It is seen that the magnetic pressure is comparable to the thermal pressure in the inner regions, but is $\sim 2\times$ higher at the outer regions of the plasma shell.

A. Local plasma heating mechanisms

The RHS terms of Eq. (3) include the plasma internal energy and the energy spent on acceleration. Here, we present calculations for the instantaneous plasma heating rates for two times during the implosion. The first RHS term in the equation separates into the compressional heating rate ($p\partial v/\partial r$) and the rate of the kinetic energy rise due to the thermal-pressure gradient ($v\partial p/\partial r$). The additional term obtained, pv/r, is small compared to the other two. The second RHS term in the equation is the heating rate due to the gradient of the electron heat flux. The third and fourth RHS terms in Eq. (3) are the Joule heating rate of electrons and the work of the Lorentz ($\mathbf{J}\times\mathbf{B}$) force, respectively. We note that the first two terms in Eq. (3) are only significant for the analysis for certain plasma regions, reflecting the energy exchange between different layers, and are zeroed out in the energy balance for the entire plasma shell.

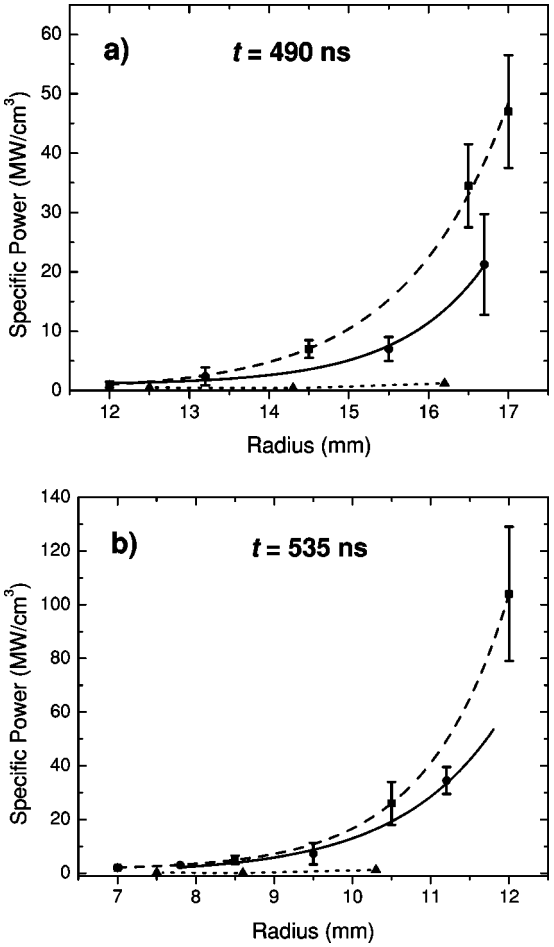

FIG. 7. Radial distribution of the energy-deposition rates in the plasma due to the Joule heating (dashed line), the compressional heating $p\partial v/\partial r$ (solid line), and the electron heat flux (dotted line), for two times during the implosion.

The terms that contribute to the rise in the internal energy ε are the compresional heating ($p\partial v/\partial r$), the Joule heating, and the electron heat flux, the calculated radial distributions of which are given in Fig. 7. In the calculations of these terms, we use the derivatives with respect to r of the smooth curves that best fit the experimental data points of T_e, n_e, and v_r, and of the curve of J_z, which is the solution of the magnetic diffusion equation [16]. For comparison, also shown in the figure are the local rates at several radial positions obtained using derivatives which are calculated based on neighboring data points, e.g., $\partial T_e/\partial r \sim \Delta T_e/\Delta r$. It is seen that near the outer boundary of the plasma shell the Joule heating dominates, while for the inner plasma layers both the compressional and Joule heating rates become nearly equal.

The electron heat flux is found to be small for all radial regions. This finding contradicts the results given in a previous study [15], where it was suggested that the electron heat flux is sufficiently significant to support the propagation of the ionization front in the plasma. This disagreement can be explained based on the overestimated electron temperature used for the analysis in Ref. [15] (T_e was not measured at the time).

B. Energy balance in the plasma

Using the instantaneous energy deposition and dissipation rates given above, it is now possible to compare the total energy deposited in the plasma E_{source} to the total (internal +kinetic) energy acquired by the plasma E_{tot}. These total energies are obtained by calculating the instantaneous values of the terms in Eq. (3) at $t=490$ and 535 ns, and integrating over the 45-ns time interval and over the radial dimension. The results are given in units of energy per unit length of the plasma shell. All the terms in Eq. (3) are calculated using the experimental data, except for the radiation cooling ε_{rad}, which is obtained from the CR calculations. For the plasma under study, the powers of both the Bremsstrahlung and the radiative-recombination continuua are by more than an order of magnitude lower than the power of the line radiation, so that ε_{rad} is calculated using the empirical expression $(1/\rho)\Sigma_i\Sigma_{j>i}n_jA_{ji}e(\tau_{ji})E_{ji}$, where $e(\tau_{ji})$ is the radiation escape probability.

The work of the Lorentz force obtained is $E_{J\times B}=18\pm5$ J/cm. This work is converted both into the plasma kinetic energy and internal energy ε (heat, ionization, and excitation). The Joule heating for this time interval yields $E_{\text{Joule}}=3\pm1$ J/cm, all converted into the plasma internal energy. For the calculations of the plasma kinetic energy $E_{\text{kin}}(t)$ the radial distributions of the plasma velocity and mass are used, the latter obtained from the distributions of n_e [13] and Z [15]. For a total mass of 11 ± 2 μg/cm the values obtained are $E_{\text{kin}}(490\text{ ns})=9\pm2$ J/cm and $E_{\text{kin}}(535\text{ ns})=22\pm3$ J/cm. The rise in the kinetic energy between these two times is then $\simeq13\pm4$ J/cm.

The internal energy $E_{\text{int}}=2\pi\int\rho\varepsilon rdr$ per unit length of the plasma shell is calculated using the time-dependent radial distributions of T_e and Z, giving 8.9 ± 2.0 and 13.6 ± 3.5 J/cm at $t=490$ and 535 ns, respectively, so that the rise is $\Delta E_{\text{int}}=4.7\pm3.0$ J/cm. The fraction of the ionization energy in ΔE_{int} is ~2.3 J/cm. For comparison, the ionization energy was also obtained from CR calculations using typical experimental values for n_e and T_e, giving ~2.8 J/cm for a 45-ns interval. The radiation losses $E_{\text{rad}}=2\pi\int\rho\varepsilon_{\text{rad}}rdr$ calculated for the 45-ns interval were found to be 1.8 ± 0.4 J/cm.

The total deposited energy $E_{\text{source}}=E_{J\times B}+E_{\text{Joule}}$ gives 21 ± 6 J/cm. The total aquired and dissipated energy $E_{\text{tot}}=E_{\text{kin}}+E_{\text{int}}+E_{\text{rad}}$ gives 19.5 ± 7.0 J/cm. One can see that $E_{\text{source}}\approx E_{\text{tot}}$, which demonstrates the consistency of the plasma parameters determined. In addition, the partition of E_{tot} provides the energy conversion efficiency during the implosion. It is seen that the kinetic energy is $\sim65\%$ of the total energy aquired by the plasma, $\sim25\%$ of the aquired energy is invested in heating and ionization, and $\sim10\%$ of the energy is radiated.

Any possible deviation of the plasma implosion geometry from a pure radial one would result in nonradial kinetic energy terms. However, the equality $E_{\text{source}}\approx E_{\text{tot}}$ shows that up to $t=535$ ns such terms are within the uncertainties of the calculations, i.e., the single-temperature 1D MHD model describes the plasma implosion sufficiently well.

VI. SUMMARY

The balance between the magnetic energy deposited in a $\sim$600-ns CO_2-puff z-pinch plasma and the energy dissipated during the implosion phase is studied. The energy deposition and dissipation rates in the plasma are determined using the measured radial distribution of the electron temperature, together with the previously observed time-dependent radial distributions of the magnetic field, the plasma density, and the particle velocities. The electron temperature is determined from ionic-level population ratios of O II–O VI that are very weakly dependent on the electron density, obtained from time-dependent, spatially resolved measurements of optically-thin spectral lines.

It was found that the work of the Lorentz force and the Joule heating constitute $\sim85\%$ and $\sim15\%$, respectively, of the energy coupled to the plasma, and that about 65% of the energy acquired by the plasma is stored in the radial ion flow. About 90% of both the energy deposition and dissipation takes place within the $\sim$1.5-mm-thick layer at the outer boundary of the 6-mm-thick plasma shell. The energy balance analysis demonstrates that for the 100-ns long interval studied (between -150 to -50 ns relative to the stagnation), the 1D model describes the plasma sufficiently well. Furthermore, the information presented here can also be used for estimating the energy stored in the plasma close to the stagnation, and thus may help in clarifying questions related to the balance between the x-ray radiation and the kinetic energy stored in the plasma radial flow raised in various z-pinch experiments.

ACKNOWLEDGMENTS

The authors wish to thank L. A. Vainshtein for his helpful comments on the atomic-physics modeling, and P. Meiri for his highly skilled technical assistance. This work was supported in part by the German-Israeli Project Cooperation foundation (DIP), by Sandia National Laboratories, USA, and by the DOE, USA.

[1] D. D. Ryutov, M. S. Derzon, and M. K. Matzen, Rev. Mod. Phys. **72**, 167 (2000).
[2] *Dense Z-Pinches*, 5th International Conference on Dense Z-Pinches, Albuquerque 23–28 June 2002, AIP Conf. Proc. No. 651, J. Davis, C. Deeny, and N. R. Pereira (AIP, Melville, NY, 2002), p. 101—126.
[3] M. A. Liberman, J. S. De Groot, A. Toor, and R. B. Spielman, *Physics of High-Density Z-Pinch Plasmas* (Springer-Verlag, New York, 1999).
[4] C. Deeney, C. A. Coverdale, and M. R. Douglas, Laser Part. Beams **19**, 497 (2001); R. B. Spielman and J. S. De Groot, *ibid.* **19**, 509 (2001).
[5] M. G. Haines, S. V. Lebedev, J. P. Chittenden, F. N. Beg, S. N. Bland, and A. E. Dangor, Phys. Plasmas **7**, 1672 (2000).
[6] C. Deeney, M. R. Douglas, R. B. Spielman, T. J. Nash, D. L. Peterson, P. L'Eplattenier, G. A. Chandler, J. F. Seamen, and K. W. Struve, Phys. Rev. Lett. **81**, 4883 (1998).
[7] T. W. L. Sanford *et al.*, Phys. Rev. Lett. **83**, 5511 (1999).
[8] L. I. Rudakov, A. L. Velikovich, J. Davis, J. W. Thornhill, J. L. Giuliani Jr., and C. Deeney, Phys. Rev. Lett. **84**, 3326 (2000).
[9] C. Deeney *et al.*, Phys. Rev. E **56**, 5945 (1997).
[10] D. L. Peterson, R. L. Bowers, K. D. McLenithan, C. Deeney, G. A. Chandler, R. B. Spielman, M. K. Matzen, and N. F. Roderick, Phys. Plasmas **5**, 3302 (1998).
[11] L. I. Rudakov and R. N. Sudan, Phys. Rep. **283**, 253 (1997).
[12] H. R. Griem, *Principles of Plasma Spectroscopy* (Cambridge University Press, Cambridge, 1997).
[13] L. Gregorian, G. Davara, E. Kroupp, V. I. Fisher, A. Starobinets, V. A. Bernshtam, and Y. Maron, Weizmann Institute Report No. WIS/23/02-June-DPP (unpublished).
[14] Yu. V. Ralchenko and Y. Maron, J. Quant. Spectrosc. Radiat. Transf. **71**, 609 (2001); R. Arad, K. Tsigutkin, Yu. V. Ralchenko, and Y. Maron, Phys. Plasmas **7**, 3797 (2000).
[15] M. E. Foord, Y. Maron, G. Davara, L. Gregorian, and A. Fisher, Phys. Rev. Lett. **72**, 3827 (1994).
[16] G. Davara, L. Gregorian, E. Kroupp, and Y. Maron, Phys. Plasmas **5**, 1068 (1998).
[17] L. Gregorian, M.Sc. thesis, Feinberg Graduate School, Weizmnann Institute of Science, 1993.
[18] W. L. Wiese, J. R. Fuhr, and T. M. Deters, J. Phys. Chem. Ref. Data Monogr. No. 7 (1996).
[19] V. P. Shevelko and L. A. Vainshtein, *Atomic Physics for Hot Plasma* (IOP, Bristol, 1993).
[20] K. L. Bell, H. B. Gilbody, J. G. Hughes, A. E. Kingston, and F. J. Smith, J. Phys. Chem. Ref. Data **12**, 891 (1983).
[21] P. Mazzotta, G. Mazzitelli, S. Colafrancesco, and N. Vittorio, Astron. Astrophys., Suppl. Ser. **133**, 403 (1998).
[22] H. R. Griem, *Plasma Spectroscopy* (McGraw-Hill, New York, 1964).
[23] A. Schulz, Ph.D. thesis, Ruhr-Universität Bochum, 1992.
[24] L. Gregorian, V. A. Bernshtam, E. Kroupp, G. Davara, and Y. Maron, Phys. Rev. E **67**, 016404 (2003).
[25] L. A. Vainshtein (private communication).
[26] J. Davis, J. L. Giuliani Jr., and M. Mulbrandon, Phys. Plasmas **2**, 1766 (1995).
[27] L. Spitzer Jr., *Physics of Fully Ionized Gases* (Interscience, New York, 1962).
[28] Ya. B. Zel'dovich and Yu. P. Raizer, *Physics of Shock Waves and High-Temperature Hydrodynamic Phenomena* (Academic, New York, 1967).